Supplementary materials

Facile Fabrication of Zeolitic Imidazolate Framework Hollow Fibre Membranes via A Novel Scalable Continuous Fluid Circulation Process

Allana Lewis[a], Ting Chen[a], Fraz Butt[a], Xiuming Wei[a], Norbert Radacsi[a], Xianfeng Fan[a], Yi Huang[a,*]

[a]School of Engineering, Institute for Materials & Processes, The University of Edinburgh, Robert Stevenson Road, Edinburgh, EH9 3FB, UK

Corresponding author: Yi Huang, E-mail: Yi.Huang@ed.ac.uk

Supplementary Text

Preparation of HF-ZifMs - Seeding and Fabrication Techniques

Aged Seeding (AS): In accordance with previous studies,[1] a mixture of metal and ligand was stirred for 25 minutes prior to introduction to the CFC system. The mixture was fed internally through the hollow fibre membrane for 25 minutes to allow for the seeding process prior to drying and a secondary growth occurring with fresh solution.

Direct Seeding (DS): Considering the loosely packaged ZIF-L crystals formed during the aged seeding synthesis, the ageing stage was replaced by direct seeding for 50 minutes. Thus, the mixture of metal and ligand was immediately introduced to the CFC system for the seeding process prior to drying and a secondary growth occurring with fresh solutions.

L→M / M→L Impregnation: to reduce the density of the seeded layers and crystal, impregnation of the metal and ligand was carried out. This occurred by applying the CFC system to the ligand solution for 50 minutes followed by the metal solution for a further 50 minutes (L→M) or vice versa (M→L). After the impregnation and drying, the secondary growth was conducted by recycling the primary ligand and metal solutions.

Ethanol Induced Fabrications: Each method of fabrication was investigated in the presence of ethanol at 5, 10 and 20 V/V% within the metal solution. Thus, seeding or impregnation was carried out under fully aqueous systems whilst the addition of ethanol was introduced to the secondary growth solution mixture.

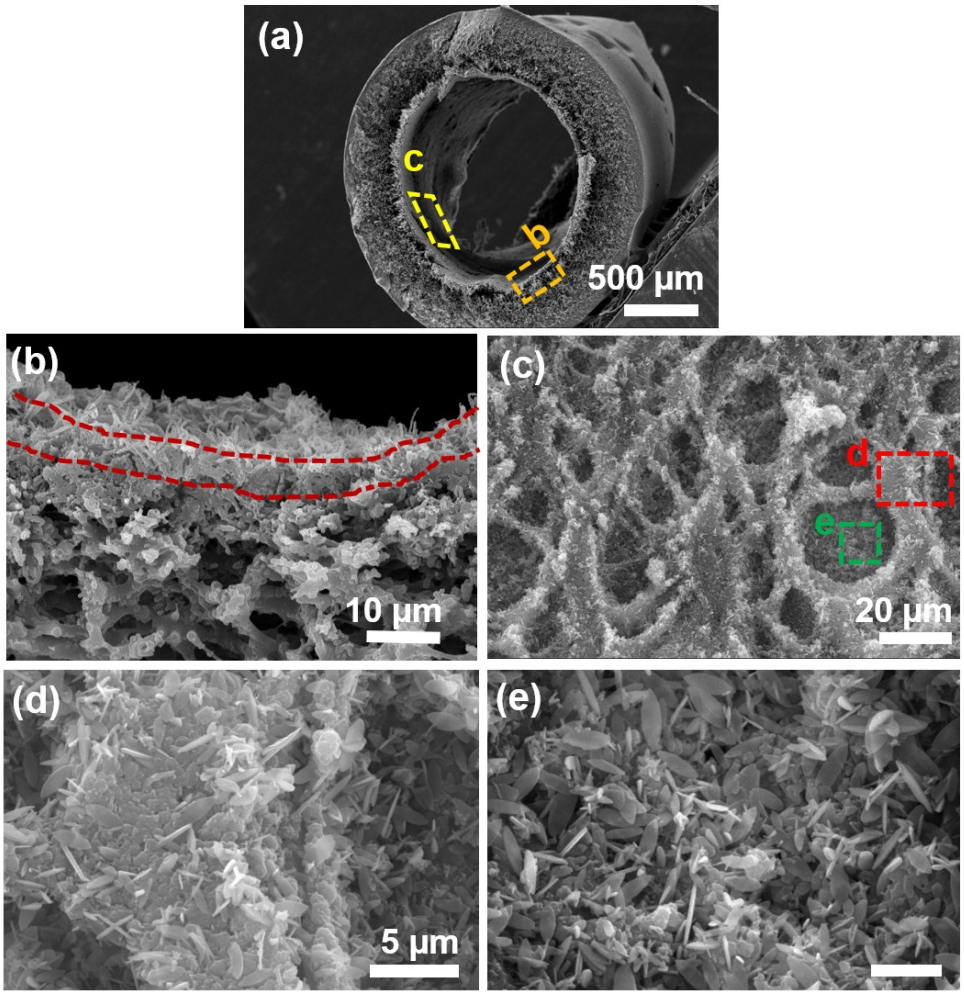

Figure S1. SEM images of the HF-ZifMs fabricated via the aged seeding (AS) synthesis route. (a)-(b) Cross-sectional SEM images of the HF-ZifMs after the aged seeding process (AS HF-ZifMs); (c)-(e) SEM images of the internal surface of the AS HF-ZifMs after secondary growth.

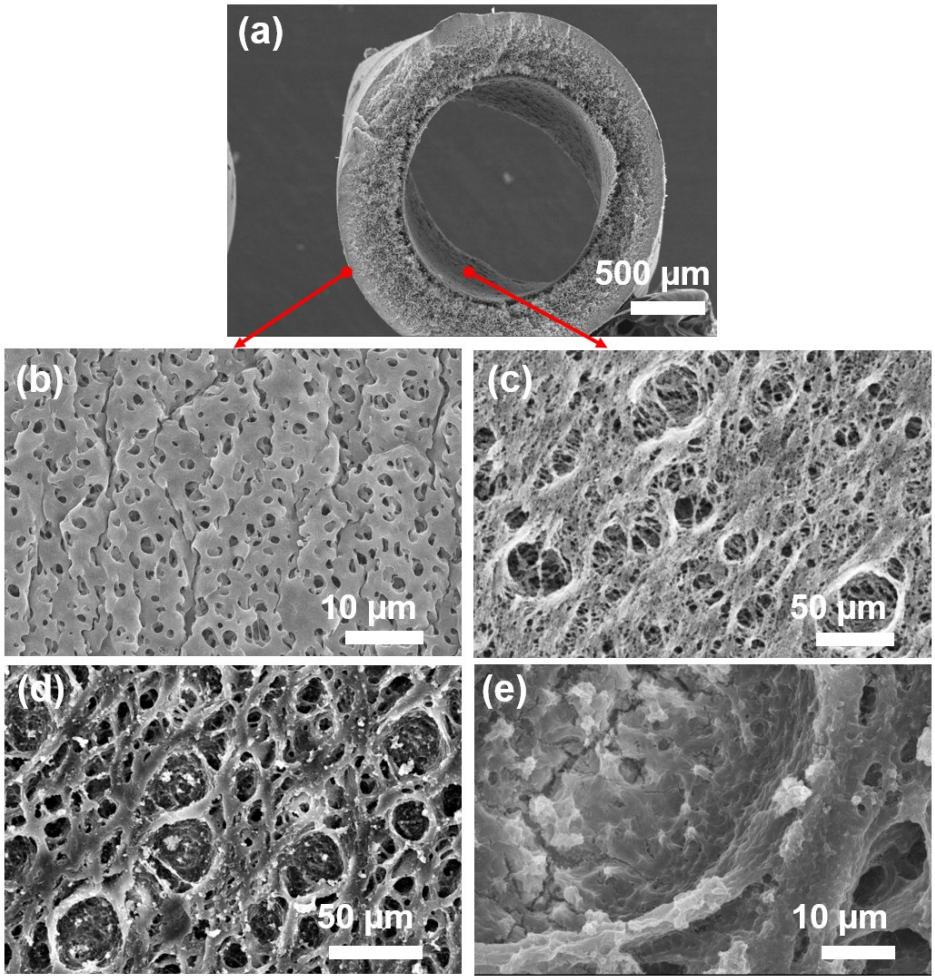

Figure S2. SEM images of the HF-ZifMs fabricated via the L→M impregnation synthesis route. (a) Cross-sectional SEM image of the bare HF; (b) SEM image of the external surface of the bare HF; (c) SEM image of the internal surface of the bare HF; (d)-(e) SEM images of the internal surface of HF after the L→M Impregnation process.

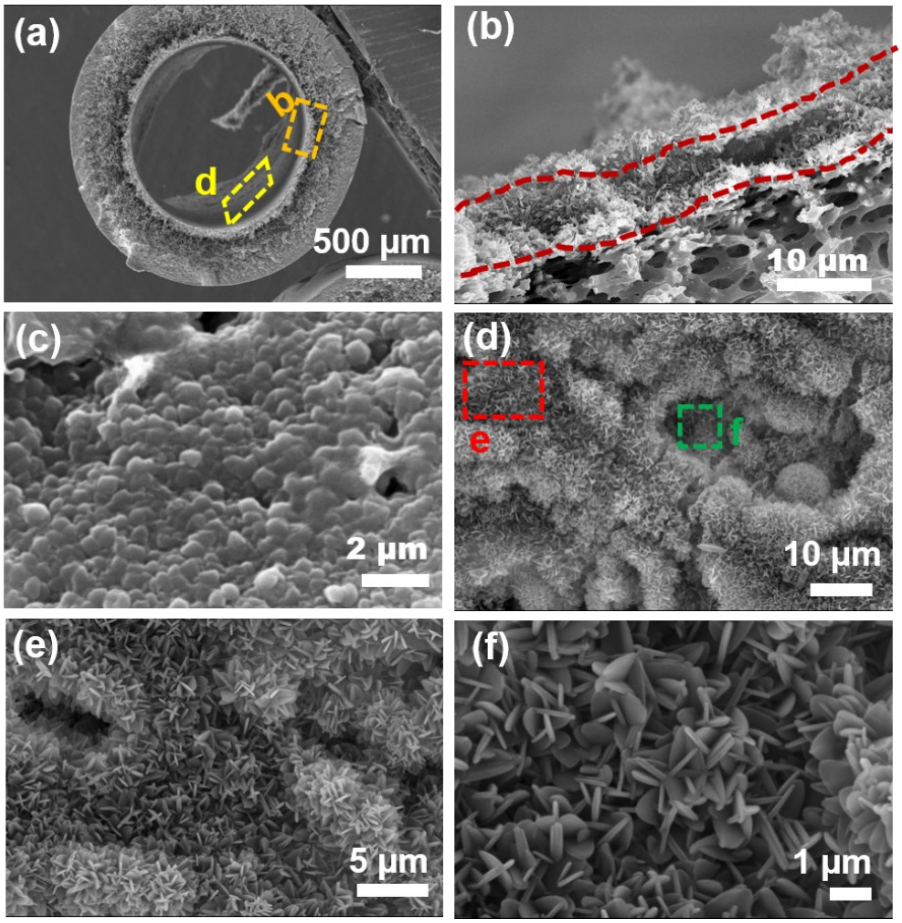

Figure S3. SEM images of the HF-ZifMs fabricated via the M→L impregnation synthesis route. (a)-(b) Cross-sectional SEM images of M→L impregnated HF-ZifMs; (c) SEM image of the internal surface of HF after M→L impregnation; (d)-(f) SEM images of the internal surface of HF after secondary growth.

As shown in Fig. S4, when the circulation order of ligand and metal solutions is M→L during the seeding procedure, a similar ZIF membrane as the L→M HF-ZifMs was obtained, but the thickness was increased to ~9 μm (Fig. S4b). The membrane also showed a dense crystal packing with vertical orientation and a rough inner surface. Compared with the L→M HF-ZifMs , the M→L impregnated membrane showed more noticeable and larger surface seeds due to an excessive amount of metal ions on the membrane surface. As a result, a thicker layer of larger ZIF crystals was produced on the inner surface of the HF-ZifMs.

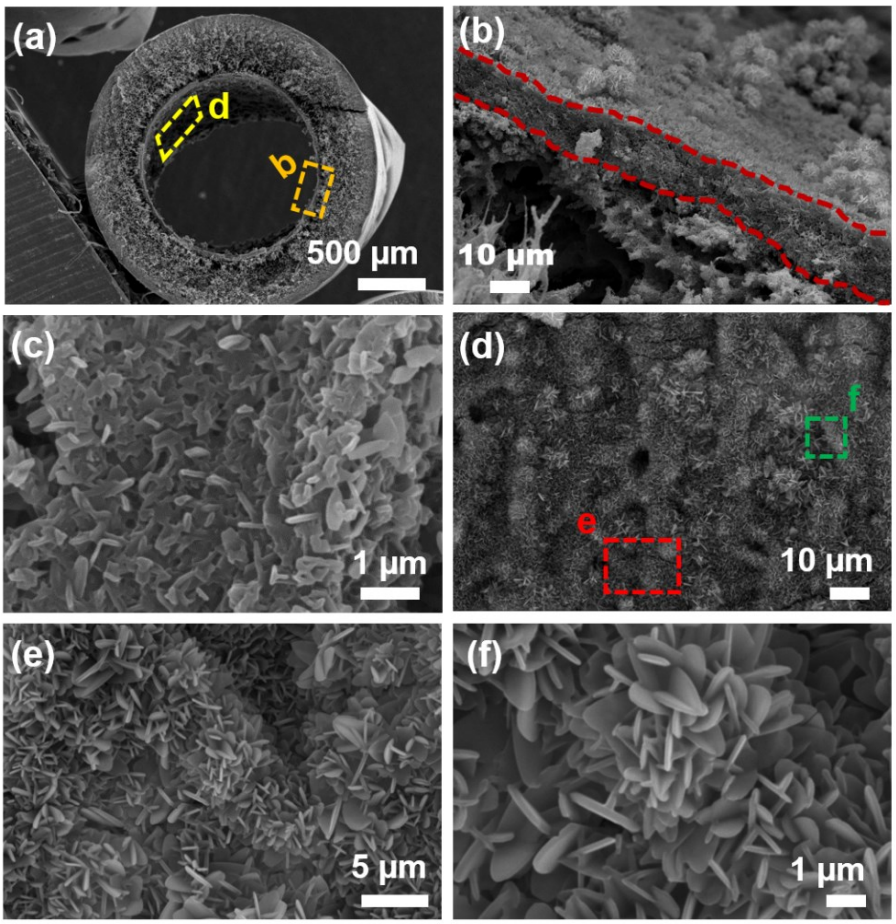

Figure S4. SEM images of the HF-ZifMs fabricated via the Direct Seeding (DS) synthesis route. (a),(b) Cross-Sectional SEM images of HF-ZifMs after the direct seeding process (DS HF-ZifMs); (c) SEM image of the internal surface of HF after seeding; (d),(f) SEM images of the internal surface of the DS HF-ZifMs after secondary growth.

As shown in Fig. S5, the HF-ZifMs fabricated via the direct seeding technique showed much denser crystal packing and thicker crystal layer as compared to the membrane fabricated using the ageing seeding technique. This is because, during the circulation of the non-aged synthesis solution, extra seed crystals were deposited onto the surface in addition to the seeds formed at the solid and liquid interfaces. The denser crystal packing and thicker ZIF-L layer of the DS HF-ZifMs suggested a less efficient oil/water separation performance than the AS HF-ZifMs.

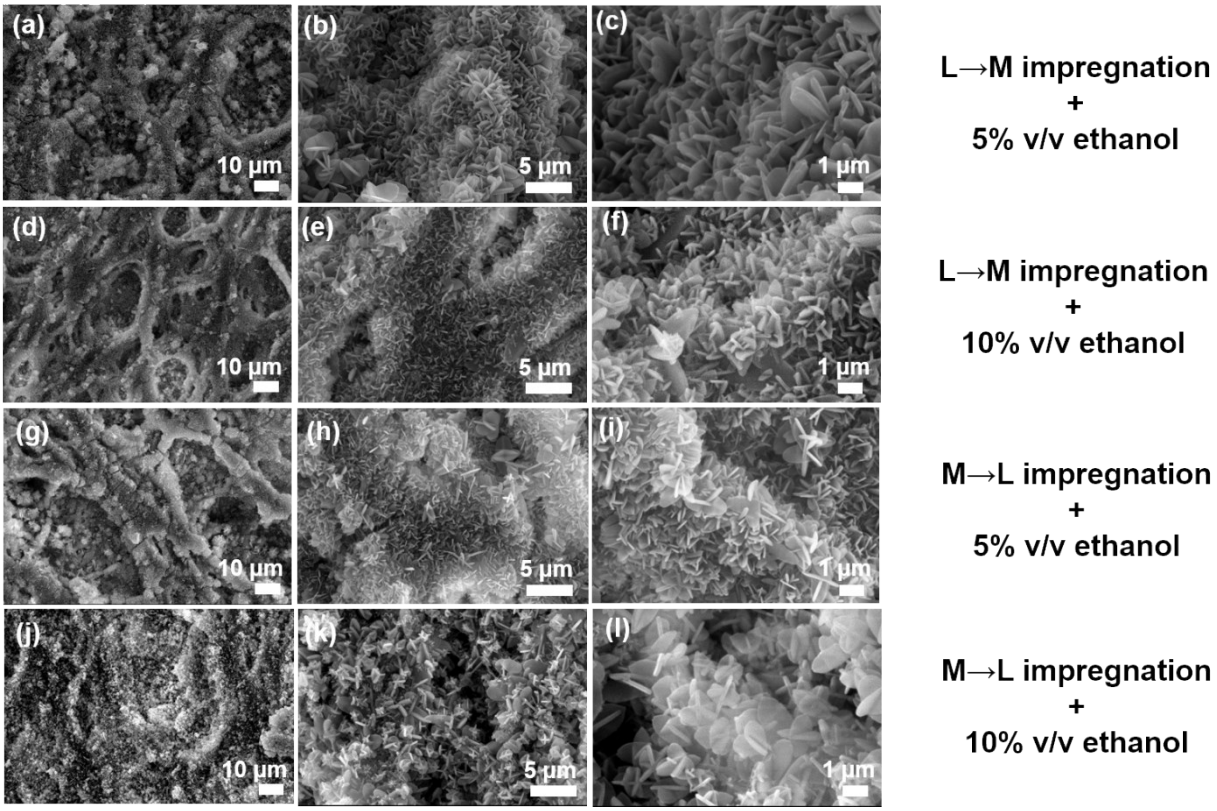

Figure S5. SEM images of HF-ZifMs prepared via impregnation CFC technique with different amount of ethanol added during the synthesis. (a)-(f) SEM images of HF-ZifMs prepared via L→M impregnation for seeding with (a)-(c) 5% (v/v), and (d)-(f) 10% (v/v) of ethanol added during the secondary growth; (g)-(l) SEM images of HF-ZifMs prepared via M→L impregnation for seeding with (g)-(i) 5% (v/v), and (j)-(l) 10% (v/v) of ethanol added during the secondary growth.

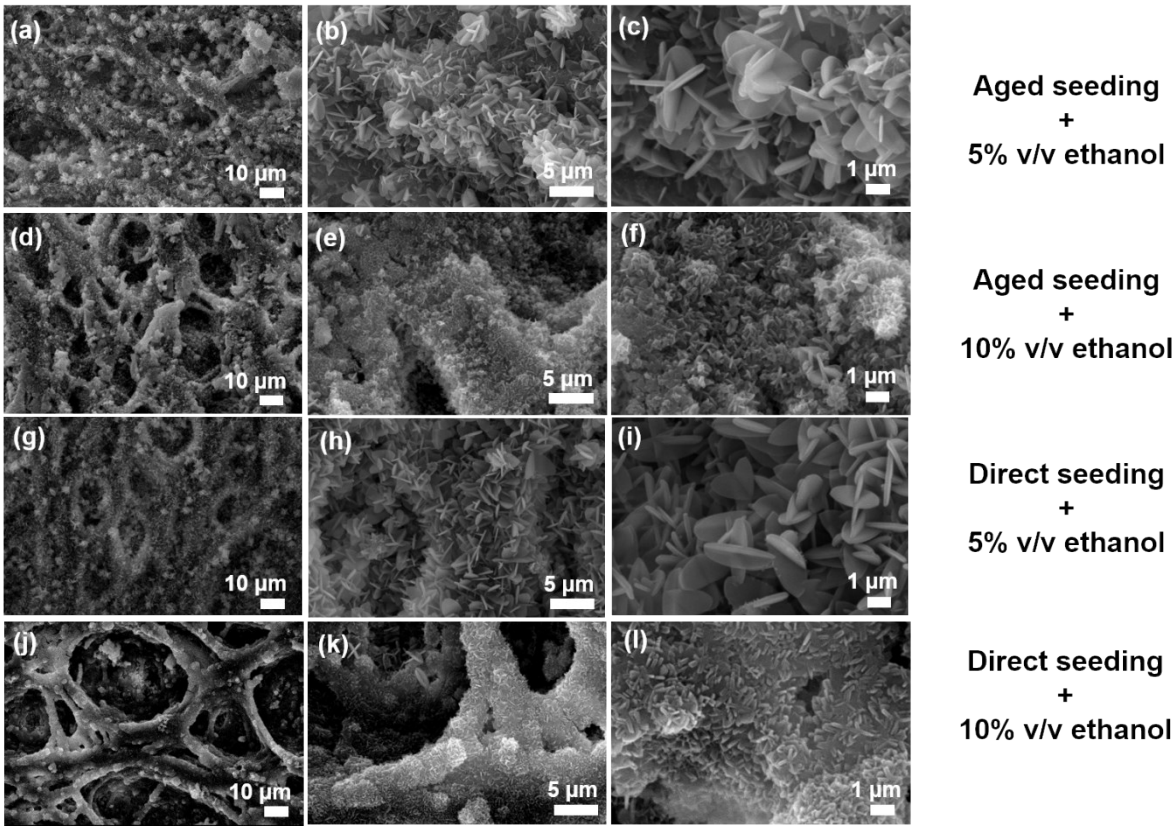

Figure S6.SEM images of HF-ZifMs prepared via seeding CFC technique with different amount of ethanol added during the synthesis. (a)-(f) SEM images of HF-ZifMs prepared via Aged Seeding with (a)-(c) 5% (v/v), and (d)-(f) 10% (v/v) of ethanol added during the secondary growth; (g)-(l) SEM images of HF-ZifMs prepared via Direct Seeding with (g)-(i) 5% (v/v), and (j)-(l) 10% (v/v) of ethanol added during the secondary growth.

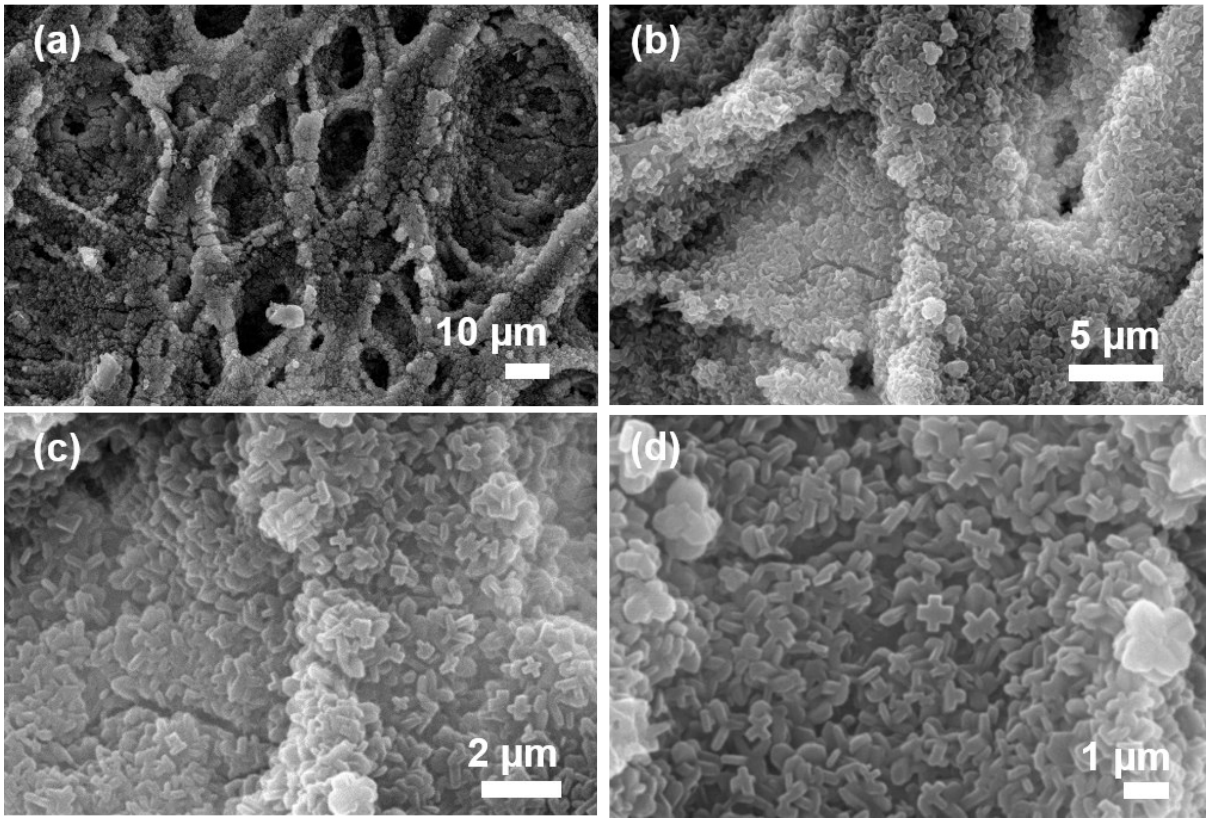

Figure S7. Influence of ethanol on crystal morphology; (a)-(d) SEM images of HF-ZifMs surface with 20% V/V ethanol added during secondary growth.

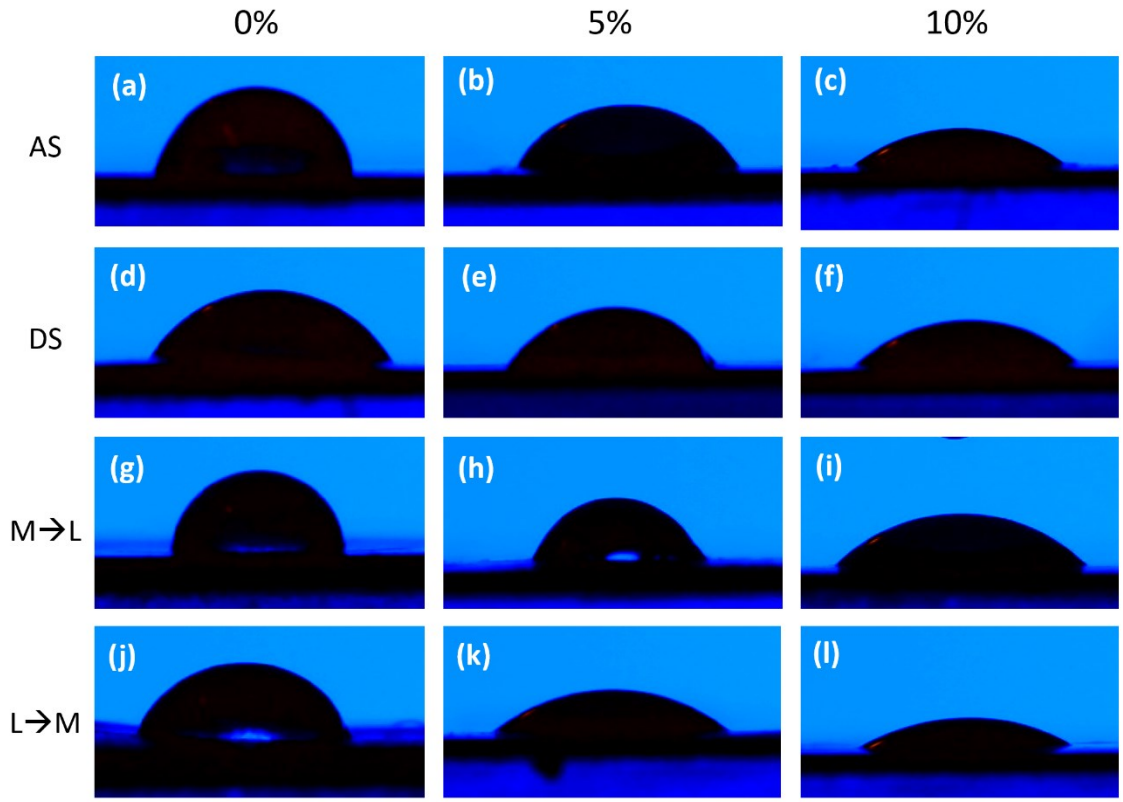

Figure S8: Surface Wettability Characterisation of HF-ZifMs with different ethanol contents; (a) AS, 0% ethanol; (b) AS, 5% ethanol; (c) AS, 10% ethanol; (d) DS, 0% ethanol; (e) DS, 5% ethanol; (f) DS, 10% ethanol; (g) M→L Impregnation, 0% ethanol; (h) M→L Impregnation, 5% ethanol; (i) M→L Impregnation, 10% ethanol; (j) L→M Impregnation, 0% ethanol; (k) L→M Impregnation, 5% ethanol; (l) L→M Impregnation, 10% ethanol.

Contact Angle Analysis for Four Fabrication Approached

According to the CA analysis, each of the fabrication approaches demonstrates a similar trend of wettability when considering the effect of ethanol. Evidently, each of the fabrication approaches at 0% V/V ethanol exhibits a hydrophilic nature with contact angles between ~82° and 67°. Despite this, the initial membrane surface, although hydrophilic, exhibited a lower degree of wettability in comparison to the 10% V/V ethanol counterparts. Contact angles were reduced to between ~50° and 45°, with the dispersion of a water droplet occurring more readily.

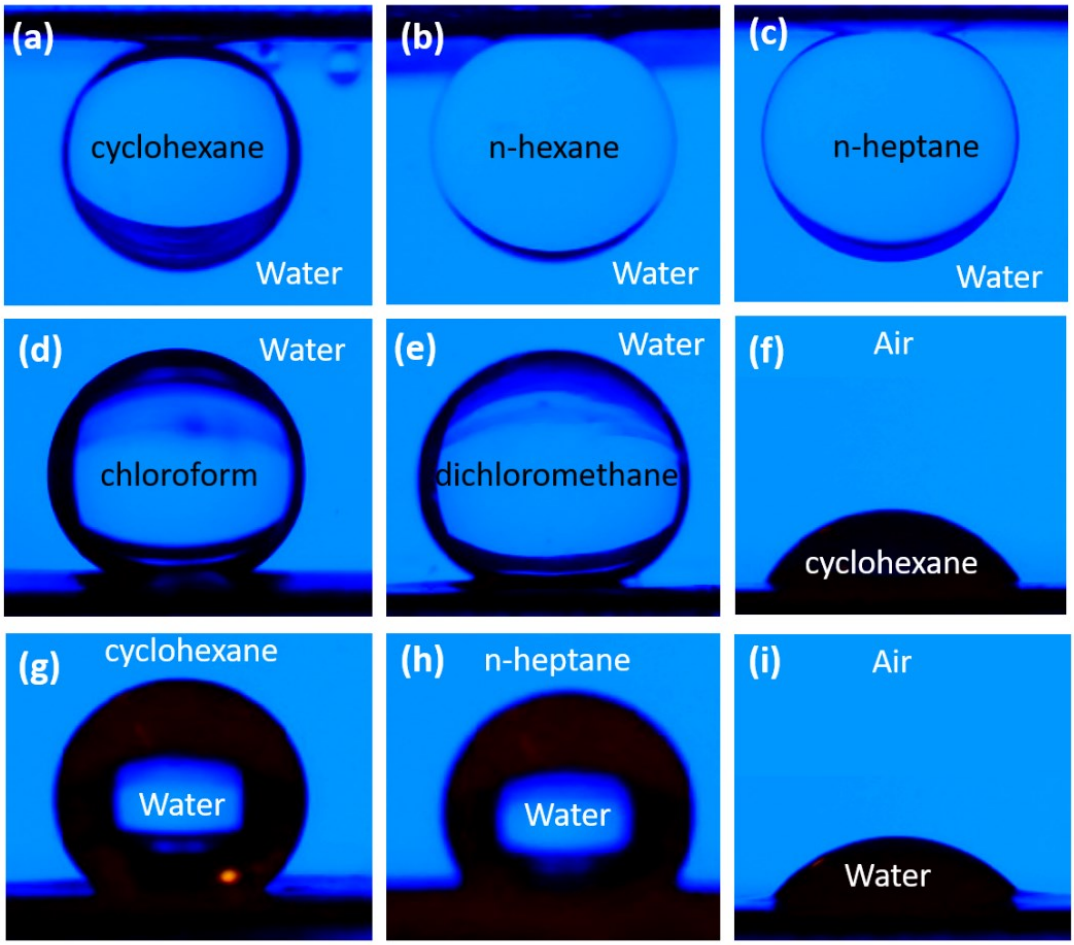

Figure S9. Surface wetting properties of L→M ZifMs; (a) UWOC angle for cyclohexane; (b) UWOC angle for n-hexane; (c) UWOC angle for n-hexane; (d) UWOC angle for chloroform; (e) UWOC angle for dichloromethane (f) cyclohexane contact angle (in air); (g) UOWC angle (in cyclohexane); (h) UOWC angle (in n-heptane); (i) WCA in air.

Contact Angle Analysis for L→ M Impregnation Technique

From the CA analysis, it is evident that the material at the surface of the membrane demonstrates both a hydrophilic and oleophilic nature which can be altered depending on the wetting stage of the membrane. Initial water permeation of the membrane allows for the membrane to be selective to water whilst rejecting oils i.e. has a superoleophobic nature upon prewetting. Likewise, if the surface is exposed to oil primarily, it acts as a water blocking barrier and only allows the passage of oils.

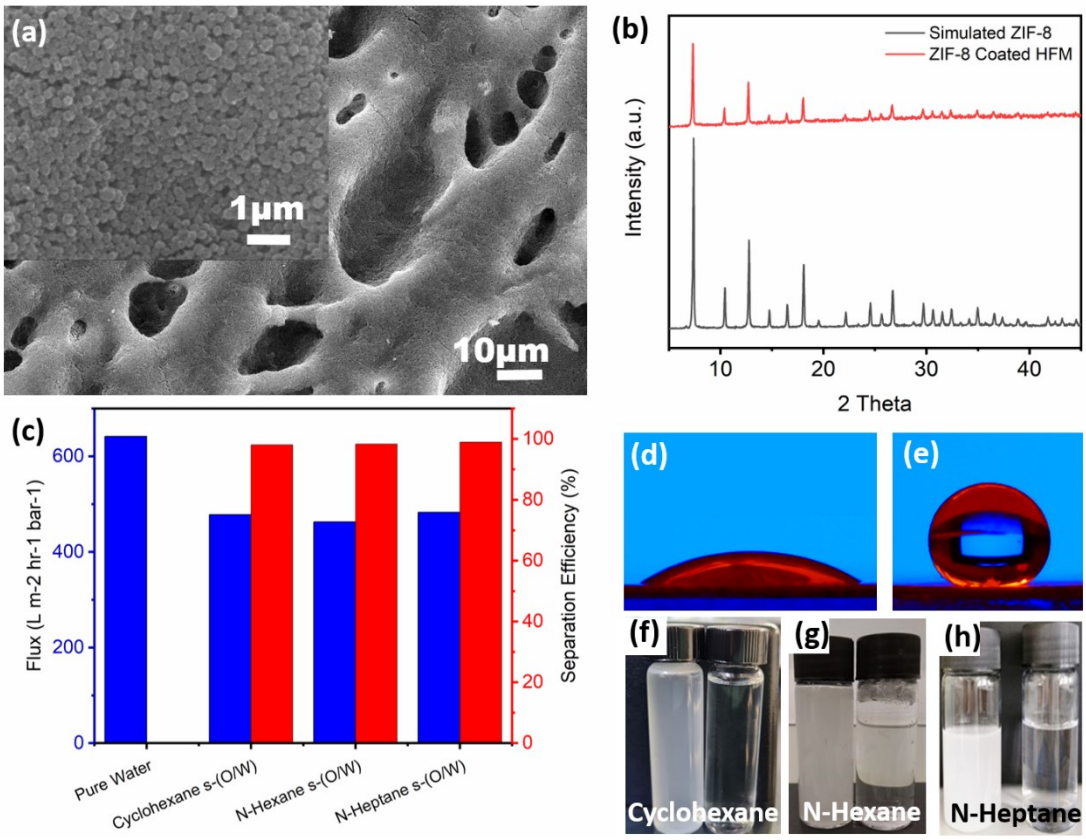

Figure S10. Characteristics of ZIF-8 based HF-ZifMs; (a) SEM images of the internal surface of the ZIF-8 based HF-ZifMs; (b) XRD pattern of flat sheet equivalent membrane of the ZIF-8 based HF-ZifMs; (c) Separation efficiency and flux of the ZIF-8 based HF-ZifMs; (d) Oil in air and (e) water in air contact angles of flat sheet equivalent membrane of the ZIF-8 based HF-ZifMs; (f) pictures showing W/O emulsions before and after separation using the ZIF-8 based HF-ZifMs.

CFC Assisted Fabrication of ZIF-8 based HF-ZifMs

Previous research has suggested a higher L: M ratio or a significant amount of solvent is required for ZIF-8 fabrications.[2] To implement this with the CFC system, a higher concentration of ligand was utilized within a mainly aqueous system containing low concentrations of solvent (similar to the previous ethanol investigation). Furthermore, to obtain ZIF-8 nuclei during the impregnation method, the impregnation was reversed to M→L, thus creating a high L: M ratio at the membrane liquid interface during impregnation.

The surface morphological analysis (Fig. S10a) and XRD analysis (Fig. S10b) of the as-synthesized material demonstrated that the fabrication of ZIF-8 decorated HF-ZifMs was successful with good crystallinity. Further analysis demonstrated that the membrane exhibits a highly oleophilic nature with an in air oil contact angle of ~47°and a hydrophobic nature with an in air-water contact angle of ~120°. Due to the highly hydrophobic nature of the materials, an oil-in-water emulsion (s-O/W) separation demonstrated a lower flux of ~475 L m^{-2} hr^{-1} $bar^{-1,}$ however, demonstrated an excellent separation performance above 98% for n-hexane in water emulsion and n-heptane in water emulsion.

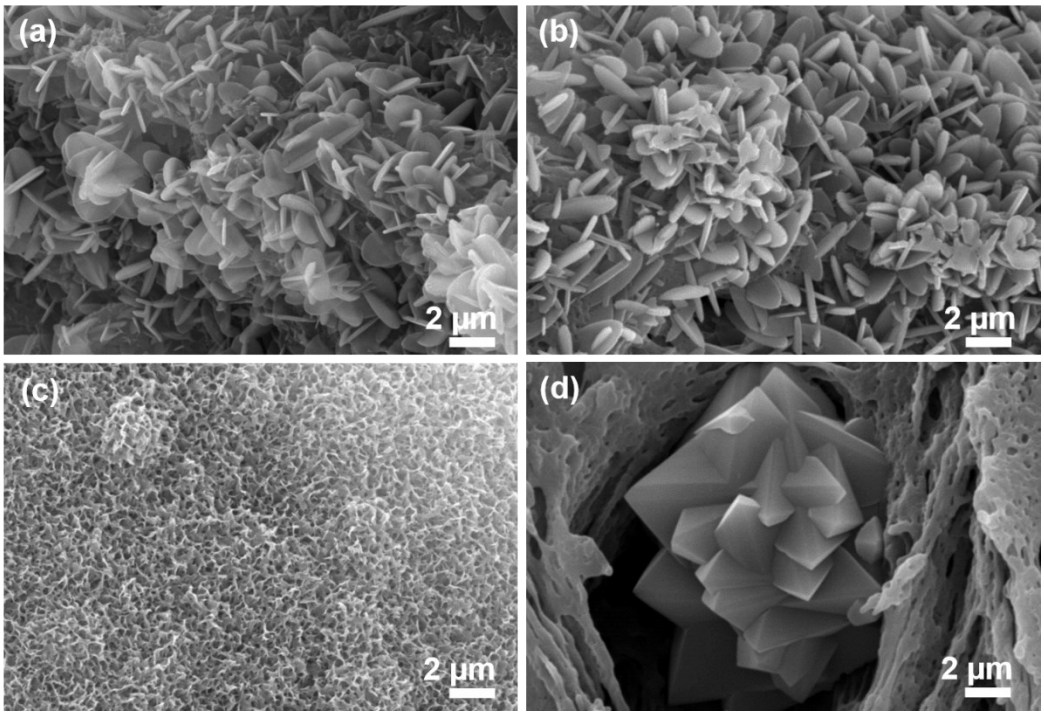

Figure S11: Hydrostability of ZIF-L crystals on L→M impregnated HF-ZifMs; SEM images of the membrane surface after (a) 0 hours, (b) 12 hours, (c) 36 hours, (d) 48 hours exposure to water.

HF-ZifMs coated with ZIF-L demonstrate a reasonable hydrostability with crystals remaining intact even after 24 hours. After such time a dissolution of the crystal occurs (36 hours) before possible recrystallisation of the materials into larger bulk crystals (48 hours). This stability can be attributed to the excellent packaging of ZIF-L crystals, therefore the stacking reduces the waters ability to attack the crystals.

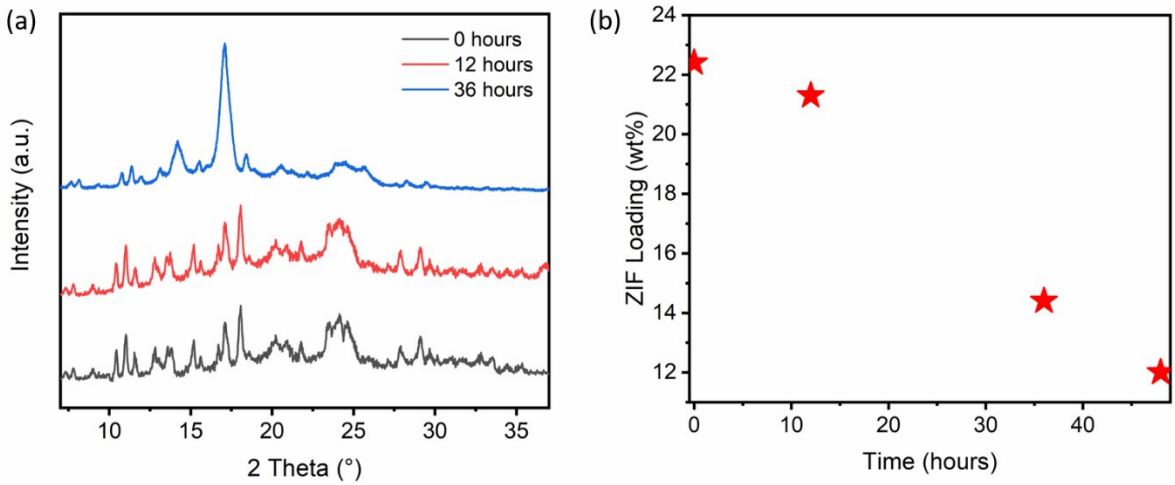

Figure S12: Hydrostability of ZIF-L crystals on L→M impregnated HF-ZifMs; (a) XRD analysis of Membranes after various water exposure durations; (b) Mass of ZIF load incorporated after various water exposure durations.

Reflecting on the SEM analysis, XRD analysis was performed on flat sheet equivalents of the HF-ZifM. In accordance with the XRD results, the ZIF materials incorporated in the membrane maintained an excellent crystallinity after 12 hours of pure water exposure, highlighting the excellent hydrostability of the materials. After 36 hours of water exposure, there is a significant decline in crystallinity with the XRD analysis exhibiting amorphous behaviours in the form of broad and low-intensity peaks. This was again supported by the change in ZIF load within the sample, displaying 22.4%, 21.3% and 14.4% at 0, 12 and 36 hours, respectively. At 48 hours a load of 12.0% was calculated. Regarding this and the SEM imaging (highlighting a lack of surface crystals), XRD analysis was not successful due to the low loading on the nylon membrane.

Table *S*1. Comparison between previously reported porous membranes for efficient oil/water separation with this work

Membrane Properties			Fabrication Method		Performance		Refs
Type of Support	**Configuration**	**Active Material**	**Total Time (hr)**	**Temp. Range (°C)**	**Normalized Flux ($L.m^{-2}.h^{-1}.bar^{-1}$)**	**Separation Efficiency (%)**	
Stainless steel mesh	Flat sheet	$Zn_2(bIm)_4$ nanosheets	~70	100-400	636	~99.9	3
Stainless steel mesh	Nanofibre coated flat sheet	Polyacrylonitrile (PAN)/ZIF-8	~25	25	900	99.9	4
Polyacrylonitrile (PAN)	Nanofibre flat sheet	UiO-66-NH_2	~64.5	40-120	~730	99	5
Polyethrtsulfone (PES)	Flat sheet	Phase inversion GO	>12	50-90	119	~99.9	6
Sulfonated polyphenylene sulfone	Tri-bore Hollow Fibre	Polyphenylenesulfone (PPSU) and sulfonated polyphenylene sulfone (sPPSU)	>120	25	~220	95.4	7
Polysulfone	Hollow Fibre	Polysulfone	>36	25	61	~99	8
Mullite Ceramic	Hollow Fibre	TiO_2	~3	25-600	150	97	9
Polyphenylene sulfone	Hollow Fibre	Sulfonated polyphenylene sulfone (sPPSU)	>72	-50 - 50	23.3	99.62	10
PVDF	Hollow Fibre	Esterified Polymers	>30	25-60	~70	98	11
Polymeric	**Hollow Fibre**	**ZIF-L**	**2.5**	**25**	**1183**	**>99.9**	**This Work**

Video S1. Demonstration of continuous crossflow oil/water emulsion separation on a hollow fibre supported ZIF-L membrane.

To better visualize the permeation through the hollow fibre supported ZIF-L membrane. The SS316 membrane module type PVM-025-1 (as shown at the bottom) was removed from the system and the membrane was mounted directly to the feed and retentate sides. As demonstrated in Video S1, the surfactant stabilized oil-in-water emulsion was pumped to create a crossflow inside the ZIF-L hollow fibre membrane. The clear permeate was captured on the outside membrane surface and collected in a clean beaker right after the emulsion separation was started. The permeate flux and oil content were then analysed to estimate the separation efficiency of the membrane sample.

Video S2. Close view of the clean water permeation from outer ZIF-L hollow fibre membrane surface.

A close view of the outer hollow fibre membrane surface showed that very clean and transparent water permeated from the inside membrane. Based on our results, the permeate collected from the best ZIF-L membrane contained less than 0.1 wt% of the oil phase.

References

1. T. Chen, A. Lewis, Z. Chen, X. Fan, N. Radacsi, A. J. C. Semiao, H. Wang, Y. Huang, Sep Purif Technol. 2020, **240**, 116647.
2. G. Liu, Z. Jiang, K. Cao, S. Nair, X. Cheng, J. Zhao, H. Gomaa, H. Wu, F. Pan, J Memb Sci. 2017, **523**, 185–96.
3. C. Ma, Y. Li, P. Nian, H. Liu, J. Qiu, X. Zhang, Sep Purif Technol. 2019, **229**, 115835.
4. Y. Cai, D. Chen, N. Li, Q. Xu, H. Li, J. He, J. Lu, J. Memb. Sci. 2017, **543**, 10–7.
5. H. Li, L. Zhu, J. Zhang, T. Guo, X. Li, W. Xing, Q. Xue, Appl Surf Sci. 2019, **476**, 61–9.
6. D. Qin, Z. Liu, H. Bai, D.D Sun, X. Song, Sci Rep. 2016, **6**, 1–12.
7. L. Luo, G. Han, T. S. Chung, M. Weber, C. Staudt, C. Maletzko, J. Memb. Science. 2015, **476**, 162-170.
8. X. Hong, X. Huang, Q. Gao, H. Wu, Y. Guo, F. Huang, F. Hua, T. Huang, D. Chen, J. Appl. Polym. Sci. 2019, **136**, 47615.
9. L. Zhu, M. Chen, Y. Dong, C. Y.Tang, A. Huang, L. Li, Water Res. 2016, **90**,277-285.
10. P. Li, S. S. Lim, J. G. Neo, R. C. Ong, M. Weber, C. Staudt, N. Widjojo, C. Maletzko, T. S. Chung, Ind. Eng. Chem. Res. 2014, **53**, 14056–14064
11. X. Zhu, W. Tu, K.H. Wee, R. Bai, J Memb. Sci. 2014, **466**, 36–44.